ELSEVIER

Journal of Power Sources 81–82 (1999) 675–679

JOURNAL OF POWER SOURCES

www.elsevier.com/locate/jpowsour

$LiCoO_2$ and $LiCo_{1-x}Al_xO_2$ thin film cathodes grown by pulsed laser ablation

J.D. Perkins [a,*], C.S. Bahn [a], P.A. Parilla [a], J.M. McGraw [b], M.L. Fu [c], M. Duncan [a], H. Yu [a], D.S. Ginley [a]

[a] *National Renewable Energy Laboratory, 1617 Cole Boulevard, Golden, CO 80401-3305, USA*
[b] *Colorado School of Mines, Golden, CO, USA*
[c] *University of Colorado, Boulder, CO, USA*

Abstract

$LiCoO_2$ and $LiCo_{0.5}Al_{0.5}O_2$ thin films have been grown by pulsed laser ablation on SnO_2-coated glass substrates. For both stoichiometries, the resultant films are dense and uniaxially textured films with the Li and Co layers parallel to the substrate. In general, to grow $LiCo_{0.5}Al_{0.5}O_2$ films, a laser flux roughly 80 mJ $pulse^{-1}$ higher than that used for $LiCoO_2$ films is required to achieve a similar deposition rate. $LiCoO_2$ films grown at $T_s = 600$°C and $p[O_2] = 2000$ mTorr have a typical grain size of $\sim$100 nm. For constant current cycling between 3.8 and 4.2 V at 5 μA, the $LiCoO_2$ films have an initial discharge capacity of $\sim$0.33 Li per $LiCoO_2$ (89 (mA h) g^{-1}) decreasing to $\sim$0.18 Li/$LiCoO_2$ (49 (mA h) g^{-1}) after 100 cycles and have a continued capacity loss of $\sim$0.25% per cycle. The $LiCo_{0.5}Al_{0.5}O_2$ films grown to date have roughly 3 times less capacity than the $LiCoO_2$ films and apparently a large asymmetry between Li extraction and reintercalation.

Keywords: $LiCoO_2$; $LiCo_{0.5}Al_{0.5}O_2$; Thin film cathodes; Li-ion batteries

1. Introduction

$LiCoO_2$ is one of the most promising cathode materials for rechargeable Li-ion batteries and is already employed in a large number of commercial Li-ion secondary batteries [1–3]. Typically, $LiCoO_2$ batteries are cycled between the discharged fully-lithiated state $LiCoO_2$ ($\sim$3.8 V vs. Li) and a charged half-delithiated state $Li_{0.5}CoO_2$ ($\sim$4.2 V vs. Li) yielding a useable capacity of $\sim$0.5 Li per transition metal ion (136 (mA h) g^{-1}). In comparison, ω-phase $Li_3V_2O_5$, which can be synthesized electrochemically from V_2O_5, has a potential capacity of 3 Li per V_2O_5 or 1.5 Li per transition metal ion [4]. Additional Li can be extracted from $Li_{0.5}CoO_2$ by increasing the charging voltage limit. In particular, Amatucci et al. find that $LiCoO_2$ can be fully delithiated to form metastable CoO_2 upon charging to 5.2 V [5]. Understanding both the mechanism for the cycling-induced capacity loss in $Li_{1-x}CoO_2$ over the restricted intercalation range $0 < \times < 0.5$ and the potential for an increased capacity upon charging to $\times > 0.5$ requires a better understanding of the intrinsic electrochemical properties of $LiCoO_2$ as well as the effects of crystallinity, grain size and morphology on the electrochemical properties of real electrodes [6–9]. In addition, thin film growth of lithium-transition-metal oxides is central to thin film and micro-battery technology development.

Increasing the cell potential is another way to improve the stored energy density, provided that the charge capacity is not degraded. Recent calculations predict that chemical substitution of aluminum for cobalt in $LiCo_{1-x}Al_xO_2$ should increase the battery voltage [10]. As aluminum is both lighter than and less expensive than cobalt, this raises the tantalizing possibility that aluminum substituted $LiCo_{1-x}Al_xO_2$ could be a cheaper, lighter, higher voltage cathode material than the current standard, $LiCoO_2$. Initial experiments, on bulk samples, do find an increased cathode voltage upon Al substitution albeit with a substantially reduced capacity [10].

In this work, we report on the pulsed laser deposition [11,12] and electrochemical characterization of $LiCoO_2$ and $LiCo_{0.5}Al_{0.5}O_2$ thin films grown on SnO_2-coated glass

* Corresponding author. Tel.: +1-303-384-6606

0378-7753/99/$ - see front matter
PII: S0378-7753(99)00266-9

substrates. For both the $LiCoO_2$ and $LiCo_{0.5}Al_{0.5}O_2$, dense uniaxially textured films with the $R\bar{3}m$ symmetry of the layered α-$NaFeO_2$ crystal structure were grown [13,14]. For both $LiCoO_2$ and $LiCo_{0.5}Al_{0.5}O_2$ films, the grain size increases with increased substrate temperature in the range 400–700°C with roughly 100 nm grains for $LiCoO_2$ films grown at 600°C and $LiCo_{0.5}Al_{0.5}O_2$ grown at 700°C. In general, the Al-substituted material must be grown roughly 100°C hotter than the stoichiometric $LiCoO_2$ to obtain similar grain size and crystallinity. For the $LiCoO_2$ films grown here, a Co_3O_4 impurity phase has been identified via Raman scattering measurements but is not observed in the X-ray diffraction measurements. This Co_3O_4 impurity phase is found to decrease with increased substrate temperature and increased oxygen partial pressure.

For constant current cycling between 3.8 and 4.2 V at 5 μA, the $LiCoO_2$ films have an initial discharge capacity of ~0.33 Li per $LiCoO_2$ (89 (mA h) g^{-1}) which decreases to ~0.18 Li/$LiCoO_2$ (49 (mA h) g^{-1}) after 100 cycles. After 100 cycles the capacity loss rate is about 0.25% per cycle. Increasing the charging limit from 4.2 to 4.6 V increases the discharge capacity by 50%. For the $LiCo_{0.5}Al_{0.5}O_2$ films, the amount of Li which can be extracted on the first charge cycle is similar to that for $LiCoO_2$. However, the subsequent capacity of the films grown to date is substantially lower, only ~0.1 Li/$LiCo_{0.5}Al_{0.5}O_2$ (33 (mA h) g^{-1}). An initial capacity loss rate of 6% per cycle decreases to 1% per cycle after 50 cycles.

2. Experimental procedures

All the films grown in this study were grown by pulsed laser ablation from nominally phase-pure stoichiometric ceramic $LiCoO_2$ or $LiCo_{0.5}Al_{0.5}O_2$ targets in a controlled atmosphere vacuum chamber using a 248 nm, 325–415 mJ $pulse^{-1}$, excimer laser operating at 10 Hz. Typically, deposition runs were 20,000 pulses long. The target and heater are parallel, on the same axis, and roughly 8.5 cm apart. During deposition, the target is rotated at 1 to 10 rpm to ensure uniform wear from the ablating beam, which strikes the target at 45°. The focused spot size is 1×3 mm at the target. To ensure good thermal contact, the SnO_2-coated 7059 glass substrates are mounted to the heater using silver paint. Crystalline $LiCoO_2$ films have been grown over the substrate temperature (T_s) range 300°C < T_s < 700°C and in the oxygen pressure ($p[O_2]$) range 50 mT < $p[O_2]$ < 2000 mTorr.

Average thickness measurements were made with a Dektak III profilometer. Corners of the SnO_2/7059 substrates were masked during growth with TiO_2 which is easily removed to allow these measurements. The metals stoichiometry was determined using inductively coupled plasma (ICP) analysis. For ICP, the $LiCoO_2$ samples were initially dissolved in 1:1 HCl:H_2O solution and then diluted to 10 vol% HCl. The phase, crystallinity and orientation of the films were determined using a four-circle Scintag diffractometer with a Cu-Kα source. The Raman scattering measurements were performed in a 180° backscattering configuration with an Ar-ion laser operating at 514.5 nm.

Electrochemical cycling experiments were conducted in an Ar-filled dry box using an Arbin Instruments four conductor battery test system with both the positive current and voltage leads connected to the cathode to mimic a standard three terminal electrochemical cell. For all tests, Li metal foil was used as both the anode and the reference voltage electrode. The electrolyte solution was either 1 M $LiClO_4$ in propylene carbonate (PC) or 1 M $LiPF_6$ in a 1:1 wt.% ethylene carbonate (EC)-dimethyl carbonate (DMC) solution. All measurements were made under constant current conditions with various voltage ranges. The specific charge capacities reported here in units of Li/$LiCoO_2$ and (mA h) g^{-1} were determined from total charge transferred along with the film thickness and area assuming a film density equal to 85% of the bulk solid density as determined from ICP and thickness measurements.

3. Results and discussion

Typical film thicknesses were 100–900 nm for $LiCoO_2$ films and 50–800 nm for $LiCo_{0.5}Al_{0.5}O_2$ films. For the $LiCo_{0.5}Al_{0.5}O_2$ films, a laser flux roughly 80 mJ $pulse^{-1}$ higher than that used for $LiCoO_2$ films is required to achieve a similar deposition rate. ICP analysis shows a Li:Co ratio of 1 ± 0.05 for the $LiCoO_2$ films but Al leaching from the 7059 glass substrates has prevented an accurate determination of the metals stoichiometry in the aluminum containing films. However, the target has a 1:1 ratio of Co:Al and in PLD film growth the stoichiometry of the film is usually close to that of the target.

Fig. 1 shows X-ray diffraction $\theta/2\theta$ spectra for a $LiCoO_2$ film grown at $T_s = 600$°C, $p[O_2] = 2000$ mTorr (curve a), for a $LiCo_{0.5}Al_{0.5}O_2$ film grown at $T_s = 600$°C, $p[O_2] = 1000$ mTorr (curve b) and for a bare SnO_2 substrate (curve c). Spectra (a) and (b) have been vertically offset for clarity. The bottom panel shows, on a linear scale, the expected $LiCoO_2$ powder diffraction pattern intensities and positions indexed to a hexagonal unit cell. Comparing the spectra for either the $LiCoO_2$ or $LiCo_{0.5}Al_{0.5}O_2$ sample with that of the bare SnO_2 substrate clearly shows that most of the observed peaks are due to the substrate. However, for both films, the (003) $LiCoO_2$ peak at ~19° is the dominant peak with a scattering intensity comparable to that for the SnO_2 substrate. The (104) $LiCoO_2$ peak at ~45°, which would be of comparable strength in a powder sample, is roughly 100 times weaker than the (003) peak for both the $LiCoO_2$ and the $LiCo_{0.5}Al_{0.5}O_2$ films. These spectra show that the films are highly (001) textured with the Li and Co layers

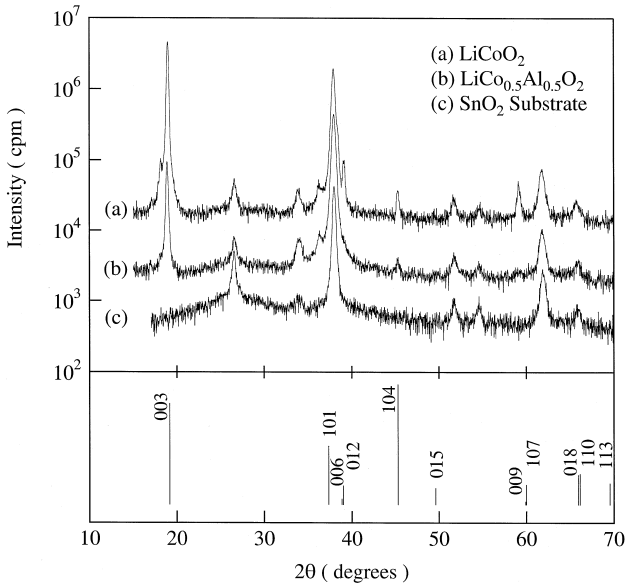

Fig. 1. Top panel: X-ray diffraction spectra for $LiCoO_2$ (a) and $LiCo_{0.5}Al_{0.5}O_2$ (b) thin films grown on SnO_2-coated 7059 glass substrates (c). The spectra are offset vertically for clarity. Bottom panel: $LiCoO_2$ powder diffraction pattern positions and intensities from JCPDS card 44-145. Vertical scale for bottom panel is linear.

parallel to the substrate surface. Pole figures (not shown) show the textured grains to have randomly oriented *a*-axes in the plane parallel to the substrate.

Fig. 2 shows SEM micrographs of a $LiCoO_2$ film (top) grown at $T_s = 600°C$, $p[O_2] = 2000$ mTorr and a $LiCo_{0.5}Al_{0.5}O_2$ film (bottom) grown at $T_s = 600°C$, $p[O_2] = 1000$ mTorr. The $LiCoO_2$ film has a grain size of ~ 100 nm whereas the $LiCo_{0.5}Al_{0.5}O_2$ film has substantially smaller grains, roughly 20–40 nm. Increasing the substrate temperature to $T_s = 700°C$ increases the grain size to 200–300 nm in $LiCoO_2$ and 50–100 nm in $LiCo_{0.5}Al_{0.5}O_2$.

Fig. 3 shows Raman scattering spectra for three representative $LiCoO_2$ films as well as for a Co_3O_4 and a $LiCo_{0.5}Al_{0.5}O_2$ film. The intensity scale for all three $LiCoO_2$ films and the $LiCo_{0.5}Al_{0.5}O_2$ is the same but that for the Co_3O_4 film has been reduced by a factor of 2.4 for clarity. The top spectra for a $LiCoO_2$ film grown at $T_s = 600°C$, $p[O_2] = 2000$ mTorr shows two well defined peaks at Raman shifts of ~ 486 cm^{-1} and ~ 596 cm^{-1} as expected for layered $LiCoO_2$ [15–17]. Whereas four peaks, inconsistent with those observed, should have been observed for $LiCoO_2$ with the cubic lithiated spinel structure [15]. In contrast, the X-ray diffraction spectra for the layered and lithiated-spinel phase of $LiCoO_2$ differ only slightly. However, taken together, the measured X-ray diffraction and Raman scattering spectra unambiguously show that the films have the layered $LiCoO_2$ structure. The spectra for the $LiCo_{0.5}Al_{0.5}O_2$ film also shows the two-line layered-structure pattern with the peaks shifted slightly up in energy to 490 and 602 cm^{-1}, respectively. However, the shifts are small relative to the peak width for the $LiCo_{0.5}Al_{0.5}O_2$ spectra.

The spectra for the $LiCoO_2$ films grown at $T_s = 400°C$, $p[O_2] = 200$ mTorr and $T_s = 400°C$, $p[O_2] = 100$ mTorr show additional peaks at ~ 690 cm^{-1} and 520 cm^{-1} with an additional weak but discernable peak at ~ 190 cm^{-1} in the latter film as well. Comparison of these spectra with that shown for the Co_3O_4 film suggests that these extra peaks may arise due to a trace Co_3O_4 impurity phase. However, no discernable Co_3O_4 peaks are apparent in the X-ray diffraction spectra. For $LiCoO_2$ films, the inset shows the strength of the 690 cm^{-1} impurity peak relative to the 596 cm^{-1} $LiCoO_2$ peak for $200°C < T_s < 800°C$ (y-axis) and 10 mTorr $< p[O_2] <$ 10,000 mTorr (x-axis). An open circle, marking each point, is filled with a solid

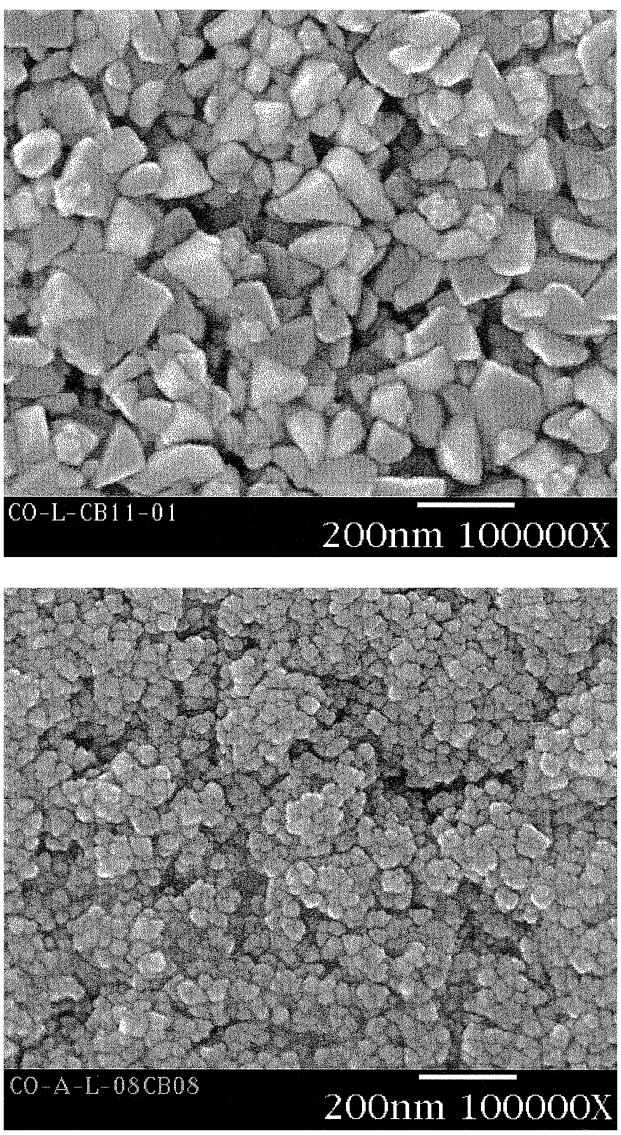

Fig. 2. Top: SEM micrograph of a $LiCoO_2$ film grown at 600°C in 2 Torr O_2 on SnO_2-coated glass. Bottom: SEM micrograph of a $LiCo_{0.5}Al_{0.5}O_2$ film grown at 600°C in 1 Torr O_2 on SnO_2-coated glass.

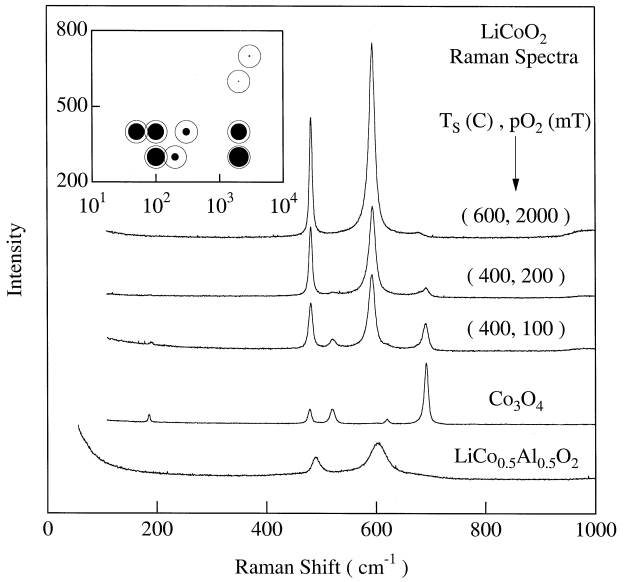

Fig. 3. Unpolarized Raman scattering spectra measured at 300 K for three representative $LiCoO_2$ thin films as well as for a Co_3O_4 and a $LiCo_{0.5}Al_{0.5}O_2$ thin film. For each $LiCoO_2$ spectra, the substrate temperature and oxygen partial pressure during film growth are shown in the figure. For $LiCoO_2$ films, the inset shows the strength of the 690 cm^{-1} impurity peak relative to the 596 cm^{-1} $LiCoO_2$ peak for 200°C < T_s < 800°C (y-axis) and 10 mTorr < $p[O_2]$ < 10,000 mTorr (x-axis). An open circle, marking each point, is filled with a solid circle whose diameter is proportional to $I[690]/I[596]$. For a fully filled circle, $I[690]/I[596] = 0.5$.

circle whose diameter is proportional to $I[690]/I[596]$. For a fully filled circle, $I[690]/I[596] = 0.5$. In general, the intensity of peak at 690 cm^{-1} relative to that for the $LiCoO_2$ peak at 596 cm^{-1} decreases with increasing $p[O_2]$ and T_s suggesting a reduced impurity content in the films grown at higher oxygen partial pressures and higher temperatures. However, for a fixed substrate temperature, 400°C for example, the relative impurity Raman scattering strength increases for $p[O_2] > 1000$ mTorr. This is due to a marked decrease in the strength of intrinsic $LiCoO_2$ Raman scattering as opposed to an increase in the impurity phase scattering. This suggests that for a given substrate temperature, the optimum oxygen pressure is determined by balancing impurity phase reduction with $LiCoO_2$ crystallinity.

The constant current charge and discharge capacities as a function of cycle number are shown in Fig. 4 for a $LiCoO_2$ film grown at $T_s = 600$°C, $p[O_2] = 200$ mTorr. The film was cycled at 5 μA between 3.8 and 4.2 V in a 1 M $LiClO_4$/PPC electrolyte. An initial discharge capacity of 0.33 $Li/LiCoO_2$ (89 (mA h) g^{-1}) decreases to 0.18 $Li/LiCoO_2$ (49 (mA h) g^{-1}) after 100 cycles. After 100 cycles, the rate of subsequent capacity loss is 0.25% per cycle. The inset shows the voltage vs. Li content for the first charge and discharge cycles. The shape of the charge and discharge curves are very similar, but only about 70% of the extracted Li can be reintercalated during discharge.

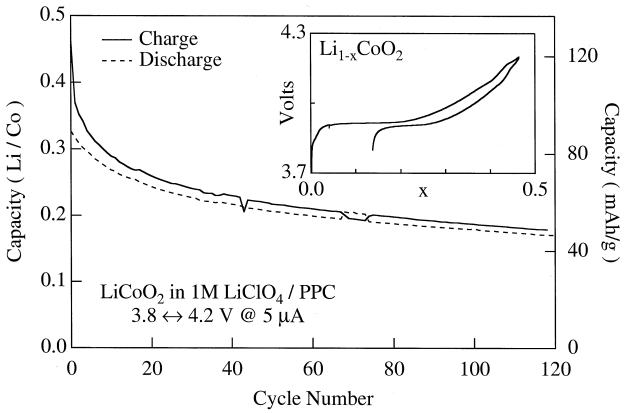

Fig. 4. Capacity, in units of Li exchanged per Co, vs. cycle number for a 3900 Å thick $LiCoO_2$ film grown at 600°C in 200 mT of oxygen. The film was cycled between 3.8 and 4.2 V vs. Li at constant current of 5 μA in a 1 M $LiClO_4$/PPC electrolyte solution. The inset shows the voltage vs. Li content for the first charge and discharge cycles.

Fig. 5 shows initial electrochemical cycling results for a $LiCo_{0.5}Al_{0.5}O_2$ film grown at $T_s = 300$°C, $p[O_2] = 100$ mTorr. The film was cycled at a constant current in 1 M $LiClO_4$/PPC. For the first 28 cycles, the film was cycled between 3.8 and 4.2 V at 5 μA. While the charge capacity of the very first charge cycle is comparable to that for a $LiCoO_2$ film, the first discharge capacity is substantially lower, about 0.1 $Li/LiCo_{0.5}Al_{0.5}O_2$ (33 (mA h) g^{-1}) compared to 0.3 $Li/LiCoO_2$ (82 (mA h) g^{-1}) as shown in Fig. 4. After 20 cycles, the cell was left in an open circuit mode for an extended time compared to the typical cycling time. The charge capacity of the next charge cycle is roughly twice that of the previous charge cycle but the subsequent discharge capacity is essentially unchanged from the previous cycle. The inset shows the voltage vs. Li content for the first two charge and discharge cycles. In comparison with $LiCoO_2$ (Fig. 4, inset), for $LiCo_{0.5}$-

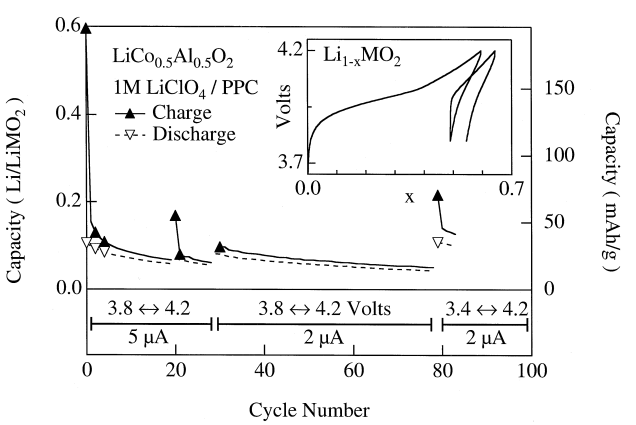

Fig. 5. Capacity, in units of Li exchanged per $LiCo_{0.5}Al_{0.5}O_2$, vs. cycle number for a 1700 Å thick $LiCo_{0.5}Al_{0.5}O_2$ film grown at 300°C in 100 mT of oxygen. The cell was cycled at constant current in 1 M $LiClO_4$/PPC. During cycling the voltage limits and current were changed as indicated in the figure. The inset shows the voltage vs. Li content for the first two charge and discharge cycles.

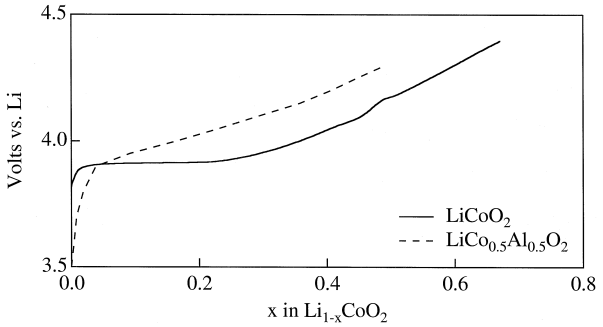

Fig. 6. Voltage vs. Li extracted on the first charge cycle for a $LiCoO_2$ film (sold line) and a $LiCo_{0.5}Al_{0.5}O_2$ film (dashed line). The 3500 Å thick $LiCoO_2$ film was grown at $T_s = 700°C$ and $p[O_2] = 2000$ mTorr while the 8100 Å thick $LiCo_{0.5}Al_{0.5}O_2$ film was grown at $T_s = 600°C$ and $p[O_2] = 1000$ mTorr.

$Al_{0.5}O_2$, the discharge does not follow the charge curve and only about 18% of the extracted Li can be reintercalated. The cycling behavior $LiCo_{0.5}Al_{0.5}O_2$ along with the large polarization of the voltage vs. charge curves relative to that for the $LiCoO_2$ films suggests a substantial asymmetry between Li extraction and intercalation dynamics in $LiCo_{0.5}Al_{0.5}O_2$. After 28 cycles, the current was reduced from 5 to 2 μA while keeping the voltage range the same as indicated in the bottom panel of Fig. 5. This factor of 2.5 reduction in the current increased the discharge capacity 40%, but the discharge capacity is still quite low compared to either $LiCoO_2$ or the first-cycle charge capacity of this same $LiCo_{0.5}Al_{0.5}O_2$ film. After 80 cycles the discharge voltage limit was reduced from 3.8 to 3.4 V which resulted in a one cycle increase in capacity of 50% but with a increased rate of capacity loss per cycle as well.

Fig. 6 compares the voltage as a function of Li extracted during the first charge half-cycle for a $LiCoO_2$ film (solid line) and a $LiCo_{0.5}Al_{0.5}O_2$ film (dashed line). During most of the charge cycle, the voltage of $LiCo_{0.5}Al_{0.5}O_2$ cathode is higher than that of the $LiCoO_2$ cathode in agreement with expectations from recent first-principles calculations [10]. However, as clear from Fig. 5, for the $LiCo_{0.5}Al_{0.5}O_2$ films grown to date, neither an increased voltage nor a reasonable capacity are realized upon discharge. We also note that the voltage plateau indicative of a two phase region for $x < 0.2$ in $Li_{1-x}CoO_2$ is not observed for $LiCo_{0.5}Al_{0.5}O_2$.

4. Summary

$LiCoO_2$ and $LiCo_{0.5}Al_{0.5}O_2$ thin films have been grown by pulsed laser ablation on SnO_2 coated glass substrates. For both stoichiometries, the resultant films are dense and uniaxially textured with the Li and Co layers parallel to the substrate. $LiCoO_2$ films grown at $T_s = 600°C$, $p[O_2] = 2000$ mTorr have a grain size of ~100 nm and reasonable electrochemical properties. The $LiCo_{0.5}Al_{0.5}O_2$ films, on the other hand, have roughly 3 times less capacity than the $LiCoO_2$ films and apparently a large asymmetry between Li extraction and reintercalation. Future film growth and characterization work will focus on elucidating the cause of, and hopefully reducing, the present decreased capacity in the aluminum substituted films.

Acknowledgements

We thank Rick Matson for the SEM micrographs presented here. This work was supported by the U.S. Department of Energy, Office of Basic Energy Sciences under contract #DE-AC36-83CH10093.

References

[1] K. Mizushima, P.C. Jones, P.J. Wiseman, J.B. Goodenough, Mater. Res. Bull. 15 (1980) 783.
[2] T.A. Hewston, B.L. Chamberland, J. Phys. Chem. Solids 48 (1987) 97.
[3] K. Ozawa, Solid State Ionics 69 (1994) 212.
[4] C. Delmas, H. Cognac-Auradou, J.M. Cocciantelli, M. Menetrier, J.P. Doumerc, Solid State Ionics, Diffusion and Reactions 69 (1994) 257.
[5] G.G. Amatucci, J.M. Tarascon, L.C. Klein, JECS 143 (1996) 1114.
[6] C. Wolverton, A. Zunger, JECS 145 (1998) 2424.
[7] J.N. Reimers, J.R. Dahn, U. von Sacken, JECS 140 (1993) 2752.
[8] G.G. Amatucci, J.M. Tarascon, L.C. Klein, Solid State Ionics 83 (1996) 167.
[9] Y.-M. Choi, S.-I. Pyun, J.-S. Bae, S.-I. Moon, J. Power Sources 56 (1995) 25.
[10] G. Ceder, Y.-M. Chiang, D.R. Sadoway, M.K. Aydinol, Y.-I. Jang, B. Huang, Nature 392 (1998) 694.
[11] M. Antaya, K. Cearns, J.S. Preston, J.N. Reimers, J.R. Dahn, J. Appl. Phys. 76 (1994) 2799.
[12] K.A. Striebel, C.Z. Deng, S.J. Wen, E.J. Cairns, JECS 143 (1996) 1821.
[13] R.J. Gummow, D.C. Liles, M.M. Thackeray, Mater. Res. Bull. 28 (1993) 235.
[14] E. Rossen, J.N. Reimers, J.R. Dahn, Solid State Ionics 62 (1993) 53.
[15] W. Huang, R. Frech, Solid State Ionics 86–88 (1996) 395.
[16] M. Inaba, Y. Iriyama, Z. Ogumi, Y. Todzuka, A. Tasaka, J. Raman Spectrosc. 28 (1997) 613.
[17] J.D. Perkins, M.L. Fu, D.M. Trickett, J.M. McGraw, T.F. Ciszek, P.A. Parilla, C.T. Rogers, D.S. Ginley, Mater. Res. Soc. Symp. Proc. 496 (1998) 329.